AIP | Journal of Applied Physics

Optoelectronic properties and interband transition of La-doped BaSnO3 transparent conducting films determined by variable temperature spectral transmittance

S. M. Xing, C. Shan, K. Jiang, J. J. Zhu, Y. W. Li, Z. G. Hu, and J. H. Chu

Citation: Journal of Applied Physics **117**, 103107 (2015); doi: 10.1063/1.4914482
View online: http://dx.doi.org/10.1063/1.4914482
View Table of Contents: http://scitation.aip.org/content/aip/journal/jap/117/10?ver=pdfcov
Published by the AIP Publishing

Optoelectronic properties and interband transition of La-doped $BaSnO_3$ transparent conducting films determined by variable temperature spectral transmittance

S. M. Xing (邢诗萌), C. Shan (单超), K. Jiang (姜凯), J. J. Zhu (诸佳俊), Y. W. Li (李亚巍), Z. G. Hu (胡志高),[a] and J. H. Chu (褚君浩)
Key Laboratory of Polar Materials and Devices, Ministry of Education, Department of Electronic Engineering, East China Normal University, Shanghai 200241, China

(Received 19 January 2015; accepted 27 February 2015; published online 12 March 2015)

Perovskite-structured $Ba_{1-x}La_xSnO_3$ ($x = 0$–0.10) films have been directly grown on (0001) sapphire substrates by a sol-gel method. Optical properties and bandgap energy of the films have been investigated by transmittance spectra from 10 K to 450 K. It indicates that these films exhibit a high transmission of more than 80% in the visible region. With increasing temperature, there is a significant bandgap shrinkage of about 0.5 eV for lightly La doping ($x \leq 0.04$) films. For heavily La doping concentration ($x \geq 0.06$), the bandgap remains nearly stable with the temperature and La composition. This is due to the fact that the lattice expansion caused by La doping is close to the saturation for the film doped with $x = 0.06$. Moreover, temperature dependent conductivity behavior shows a similar pattern, which suggests that the doping concentration of La-doped $BaSnO_3$ (BLSO) films has a saturated state. The La introduction can modify the Sn 5*s*-O 2*p* antibonding state and the nonbonding O 2*p* orbital, which remarkably affect the electronic bandgap of the BLSO films. © *2015 AIP Publishing LLC*. [http://dx.doi.org/10.1063/1.4914482]

I. INTRODUCTION

Transparent conducting oxides (TCOs), combining a high optical transparency in visible wavelengths with high electrical conductivity and low conductive resistivity, have a wide range of applications in many fields such as solar energy, flat panel displays, and smart coatings.[1,2] Many oxide materials, such as ZnO, SnO_2, and In_2O_3, have been widely investigated. However, these well-known material systems still have some limitations such as instability of oxygen content, fatigue, and degradation. Thus, there has been a challenge to find an appropriate alternative transparent material to exhibit better properties. Fortunately, perovskite-structured oxides represent an important class of transparent materials due to good properties such as ferroelectricity, ferromagnetism, superconductivity, and piezoelectricity.[3–6] At the same time, multilayer structure of perovskite materials for microelectronic materials and devices also have great potential applications. Therefore, there has been a great necessity for the further study on its structure and the physical mechanism.

Alkaline earth stannates with the general formula $RSnO_3$ (R = Ba, Sr, and Ca) are important transparent materials due to interesting physical properties and perovskite structures.[7–9] Here, R is generally rare earth ions or alkaline earth elements. Among $RSnO_3$, $BaSnO_3$ (BSO) is an ideally cubic perovskite-type oxide. It behaves as an *n*-type semiconductor, which has a wide bandgap and exhibits a high transmittance of more than 85% in the visible region. $BaSnO_3$ has been used in various fields such as physical sensors, epitaxial structure, and future photovoltaic technology.[10–13] Recent research shows that BSO doped with lanthanum (La) shows great advantages of thin film formation. It has been reported that La-doped $BaSnO_3$ (BLSO) has a high mobility of 320 $cm^2\ V^{-1}\ s^{-1}$ for carrier concentration of $8 \times 10^{19}\ cm^{-3}$ and a bandgap of more than 4 eV, which is significantly larger than those from typical transparent conductive oxides.[14,15] Consequently, BLSO is a promising candidate for transparent conductor applications and epitaxial multilayer devices. Recently, Shan *et al.* have explored an intrinsic relationship between optical properties and La concentration for BLSO system.[16,17] There have also been some works on electronic band structure and infrared optical phonons of BLSO bulk material.[18] However, temperature dependence of optical properties and bandgap energy of BLSO film has not been studied to date. Therefore, it is desirable for us to conduct a more thorough study on the spectral behavior of high-quality BLSO layer system.

In this article, we reported that the transmittance spectra of $Ba_{1-x}La_xSnO_3$ films with La concentration from $x = 0$ to 0.10 grown on (0001) sapphire substrates by the sol-gel method. Temperature dependence of electronic transitions and optical properties has been systematically discussed. It was found that La concentration has significant effects on the bandgap energy and dielectric response. Experimental and theoretical results have been provided for a better understanding on the physical properties, especially those which can be determined in the electronic orbit and lattice structure.

II. EXPERIMENTAL DETAILS

The transmittance spectra of the BLSO films with La concentration at $x = 0.00$, 0.02, 0.04, 0.06, 0.08, and 0.10

[a]Author to whom correspondence should be addressed. Electronic mail: zghu@ee.ecnu.edu.cn. Tel.: +86-21-54345150. Fax: +86-21-54345119.

were recorded by a double beam ultraviolet-infrared spectrometer (PerkinElmer UV/VIS Lambda 950) at the photon energy of 2650–190 nm (0.5–6.5 eV) with an interval of 2 nm. The samples are mounted on a cold stage of an optical cryostat (Janis SHI-4-1) and a heating stage (Bruker A599) for low temperature and high temperature experiments, respectively. Note that the temperature can be varied from 10 K to 450 K. For the electrical properties, two-point measurement was applied to measure the resistivity of BSLO films. A Keithley 6430 source meter was applied to provide an external direct current with the value of 100 nA to the sample via platinum electrodes. Correspondingly, the resistance value can be recorded.

To extract the dielectric functions and physical parameters of the BLSO films, the experimental spectra were analyzed by a three-layered structure (air/BLSO/substrate). At near-normal-incidence configuration, the following form describes the transmittance coefficient $t = t_{01}t_{12}e^{-i\delta}/(1 + t_{01}t_{12}e^{-2i\delta})$, where the partial transmittance coefficient t_{01} (vacuum-film) and t_{12} (film-substrate) are written as $t_{i,i+1} = 2\sqrt{\tilde{\varepsilon}_i}/(\sqrt{\tilde{\varepsilon}_i} + \sqrt{\tilde{\varepsilon}_{i+1}})$ and the phase factor for the film with thickness d is described by $\delta = 2\pi d\sqrt{\tilde{\varepsilon}_1}/\lambda$. Here, λ is the incident wavelength, and the dielectric functions of vacuum, the film and the substrate are $\tilde{\varepsilon}_0\,(=1)$, $\tilde{\varepsilon}_1$, and $\tilde{\varepsilon}_2$, respectively. Thus, the spectral transmittance can be readily obtained from $T = \mathrm{Real}(\sqrt{\tilde{\varepsilon}_2})tt^*$. It should be noted that the absorption from the substrate must be taken into account to calculate the transmittance of the film-substrate system. For the undoped film, the spectra were fitted with double Tauc-Lorentz (TL) oscillators. For the doped films, the transmittance can be modeled with double Tauc-Lorentz oscillators and a Drude oscillator. The imaginary part of the Tauc-Lorentz model can be written as $\tilde{\varepsilon}_1(E) = \varepsilon_\infty + \frac{2}{\pi}P\int_0^\infty \frac{\xi\varepsilon_2(E)}{\xi^2 - E^2}d\xi$, and the real part is given by the Kramers-Krönig transformation $\tilde{\varepsilon}_2(E) = \frac{AE_0C(E-E_g)^2}{(E^2-E_0^2)^2+C^2E^2}\frac{1}{E}(E > E_g)$, $\varepsilon_2(E) = 0(E \le E_g)$. Here, A is the transition matrix element, E_0 is the peak transition energy, C is the broadening term, E_g is the bandgap energy, and ε_∞ is the high frequency dielectric constant.[19] The Drude model describes free carrier effects on the dielectric response, whose form is a Lorentz model with zero center energy. It can be written as $\tilde{\varepsilon}(E) = -\frac{D_nB_r}{E^2+iB_rE}$. Here, D_n is the oscillator strength and B_r is the broadening term.

III. RESULTS AND DISCUSSION

A. NIR-UV transmittance spectra and dielectric functions

The insets of Figure 1 show the experimental transmittance spectra and the best-fitting results of the BLSO films, which exhibit a high transparency of more than 80% in the visible region. The best-fitting parameter values of the Tauc-Lorentz and Drude model with the error bars are summarized in Table I. In the high-energy region (around 4.0 eV), the transmission decreases greatly. The spectral loss can be resulted from the following physical processes: the lattice expansion and lattice vibrational state. Figure 1 shows the transmittance spectra of the BLSO films from 10 K to 450 K. As the temperature increases, the distance between the

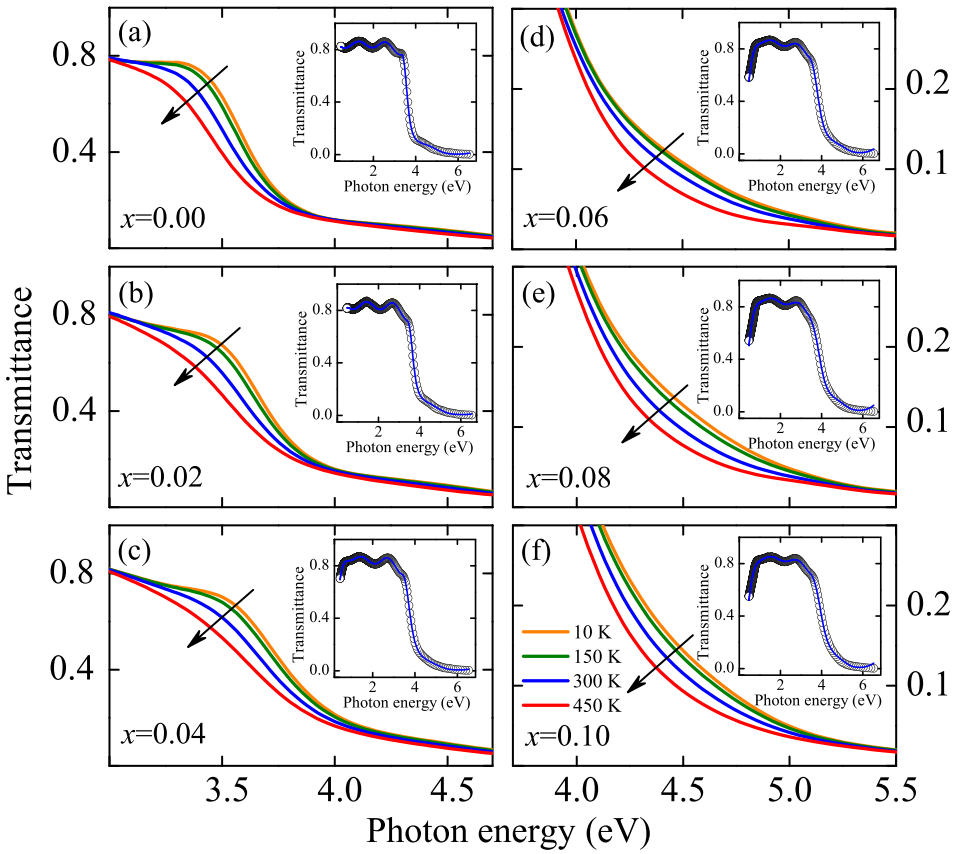

FIG. 1. The transmittance spectra near the absorption region from the BLSO films with different La doping concentration. The arrows show that the absorption edges of the BLSO films present a red-shift trend with the temperature. Note that experimental transmittance spectra (dotted lines) at 10 K and the best-fitting results (solid lines) of the BLSO films were shown in the insets.

TABLE I. Parameters of the Tauc-Lorentz and Drude dielectric function model for $Ba_{1-x}La_xSnO_3$ films determined from the simulation of the transmittance spectra. The 90% reliability is given in parentheses.

Samples	$x=0.00$			$x=0.02$			$x=0.04$			$x=0.06$			$x=0.08$			$x=0.10$		
T (K)	10	300	450	10	300	450	10	300	450	10	300	450	10	300	450	10	300	450
ε_∞	2.38	3.15	3.03	3.41	3.18	3.10	3.22	3.12	3.00	2.97	2.72	2.67	2.62	2.54	2.21	2.70	2.41	2.29
	(0.06)	(0.01)	(0.02)	(0.02)	(0.01)	(0.02)	(0.02)	(0.01)	(0.03)	(0.02)	(0.11)	(0.21)	(0.03)	(0.03)	(0.01)	(0.03)	(0.05)	(0.02)
A_1 (eV)	28.3	34.1	51.5	17.6	23.3	36.5	19.1	24.5	37.5	12.8	16.3	17.8	11.1	12.3	14.2	11.6	15.1	18.2
	(0.55)	(0.45)	(0.61)	(0.43)	(0.24)	(0.71)	(0.59)	(0.60)	(0.63)	(0.82)	(0.18)	(0.21)	(0.14)	(0.21)	(0.38)	(0.54)	(0.84)	(0.32)
E_{01} (eV)	3.77	3.56	3.32	3.86	3.68	3.42	3.95	3.74	3.41	4.17	4.10	4.01	4.20	4.13	4.04	4.22	4.14	4.06
	(0.01)	(0.01)	(0.02)	(0.02)	(0.01)	(0.02)	(0.01)	(0.01)	(0.05)	(0.02)	(0.02)	(0.02)	(0.01)	(0.01)	(0.01)	(0.02)	(0.02)	(0.01)
C_1 (eV)	0.99	0.97	0.86	0.84	0.96	1.01	1.20	1.24	1.26	1.38	1.60	1.56	1.42	1.47	1.48	1.39	1.44	1.45
	(0.02)	(0.01)	(0.01)	(0.02)	(0.01)	(0.02)	(0.03)	(0.02)	(0.05)	(0.10)	(0.12)	(0.11)	(0.15)	(0.15)	(0.15)	(0.18)	(0.17)	(0.17)
E_{g1} (eV)	3.24	3.24	3.24	3.26	3.26	3.26	3.30	3.30	3.30	3.21	3.21	3.21	3.19	3.19	3.19	3.39	3.39	3.39
	(0.01)	(0.01)	(0.01)	(0.01)	(0.01)	(0.01)	(0.01)	(0.01)	(0.01)	(0.04)	(0.04)	(0.04)	(0.07)	(0.07)	(0.07)	(0.06)	(0.06)	(0.06)
A_2 (eV)	17.9	7.35	9.10	7.85	10.2	12.0	6.00	7.98	9.72	1.89	1.79	1.59	1.96	1.83	1.62	3.18	2.90	2.72
	(0.94)	(0.15)	(0.39)	(0.23)	(0.12)	(0.43)	(0.24)	(0.19)	(0.47)	(0.15)	(0.15)	(0.15)	(0.19)	(0.19)	(0.19)	(0.26)	(0.24)	(0.25)
E_{02} (eV)	5.78	5.82	5.76	5.65	5.79	5.80	5.80	5.83	5.78	5.84	5.81	5.83	5.81	5.81	5.81	5.77	5.71	5.66
	(0.03)	(0.04)	(0.11)	(0.03)	(0.02)	(0.09)	(0.04)	(0.04)	(0.12)	(0.06)	(0.07)	(0.08)	(0.08)	(0.08)	(0.09)	(0.07)	(0.07)	(0.07)
C_2 (eV)	0.47	2.70	3.74	1.97	3.18	4.11	1.88	2.79	3.72	1.32	1.46	1.51	1.49	1.53	1.55	1.69	1.72	1.79
	(0.03)	(0.04)	(0.19)	(0.06)	(0.03)	(0.18)	(0.06)	(0.06)	(0.25)	(0.12)	(0.14)	(0.16)	(0.17)	(0.18)	(0.20)	(0.15)	(0.16)	(0.19)
E_{g2} (eV)	2.23	2.23	2.23	2.37	2.37	2.37	2.38	2.38	2.38	1.05	1.05	1.05	0.97	0.97	0.97	1.62	1.62	1.62
	(0.01)	(0.01)	(0.01)	(0.01)	(0.01)	(0.01)	(0.02)	(0.02)	(0.02)	(0.26)	(0.26)	(0.26)	(0.41)	(0.41)	(0.41)	(0.19)	(0.19)	(0.19)
D_n (eV)	…	…	…	2.41	2.13	2.61	8.57	7.26	8.65	7.09	6.82	7.37	7.28	6.56	7.60	5.07	5.34	5.83
				(0.16)	(0.05)	(0.12)	(0.20)	(0.07)	(0.18)	(0.53)	(0.49)	(0.53)	(0.76)	(0.69)	(0.79)	(0.48)	(0.44)	(0.47)
B_r (eV)	…	…	…	0.08	0.09	0.08	0.08	0.09	0.07	0.11	0.12	0.11	0.12	0.13	0.11	0.16	0.15	0.14
				(0.01)	(0.01)	(0.01)	(0.01)	(0.01)	(0.01)	(0.01)	(0.01)	(0.01)	(0.01)	(0.01)	(0.01)	(0.01)	(0.01)	(0.01)

lattices gradually increases and the lattice wave frequency changes with the crystal volume. The phenomenon is due to the fact that there has been an upward movement of the valence band bottom as the electrons of the semiconductor gain more energy. Another factor is the variation of the state of lattice vibrations with the temperature, which results in the variation of the phonon excitation state. Thus, it leads to the electron-phonon coupling and the variation in the perturbation of energy band. Both of these effects cause a relative movement of the bandgap edge. Note that these mechanisms become increasingly important for the photon energy near the absorption region. The absorption edge presents a typical red-shift trend with the temperature, which can be observed from most of semiconductors and dielectrics. For the specific variation of the absorption edge, there has been a difference between lightly La doping ($x \leq 0.04$) and heavily La doping ($x \geq 0.06$). For the La concentration at $x = 0.00$, 0.02, and 0.04, temperature dependent variations in the absorption edge position are around 3.5 eV. For the La concentration at $x = 0.06$, 0.08, and 0.10, however, the variations are located at about 4.3 eV.

The evaluated dielectric function $\varepsilon = \varepsilon_1 + i\varepsilon_2$ of the BLSO films are shown in Figure 2. The maximum position of dielectric function has a red-shift trend with increasing temperature. The real part ε_1 in the low photon energy increases with the temperature, while it shows an opposite trend at the high photon energy side. The imaginary part ε_2 shows the similar trend as the real part. Note that both of the critical point energies, in general, show a red shift with increasing temperature, which can be attributed to the thermal expansion of the lattice and renormalization of the band structure by electron-phonon interaction.[20] From the imaginary part ε_2, there have been two obvious electronic transitions in BLSO materials. The first ascent of the absorption edge is around 3.5 eV and the second is around 4.3 eV, which indicates that there has been another strong absorption. In terms of the electronic band structure, the conduction band minimum (CBM) of $BaSnO_3$ originates from the Sn 5*s*-O 2*p* antibonding state. The valence band maximum (VBM) is derived from the nonbonding O 2*p* orbital.[21] Note that the CBM and VBM are situated in the Γ point and the R point, respectively. The first optical absorption (E_{01}) is due to the direct transition from VBM to CBM at Γ point.[22] The second absorption (E_{02}) edge implies another energy minimum in the conduction band, which is located in the R point. The electrons can be excited from the valence band to the conduction band at R point if the energy is large enough.

From Figs. 2(a) and 2(b), we can note that the parameter ε_1 increases and ε_2 decreases sharply with increasing photon energy in the near-infrared region for La doped with $x = 0.06$. However, the parameters remain stable in the same region for the undoped film. This is because of the free carrier absorption. With increasing the La concentration, more free electrons have been provided inside the films. When the photon energy is not large enough, it will not cause the band transition or exciton absorption. Thus, the transition and absorption occur in the same energy band. From Figs. 2(c)–2(h), we can see that the trend of the dielectric functions with the

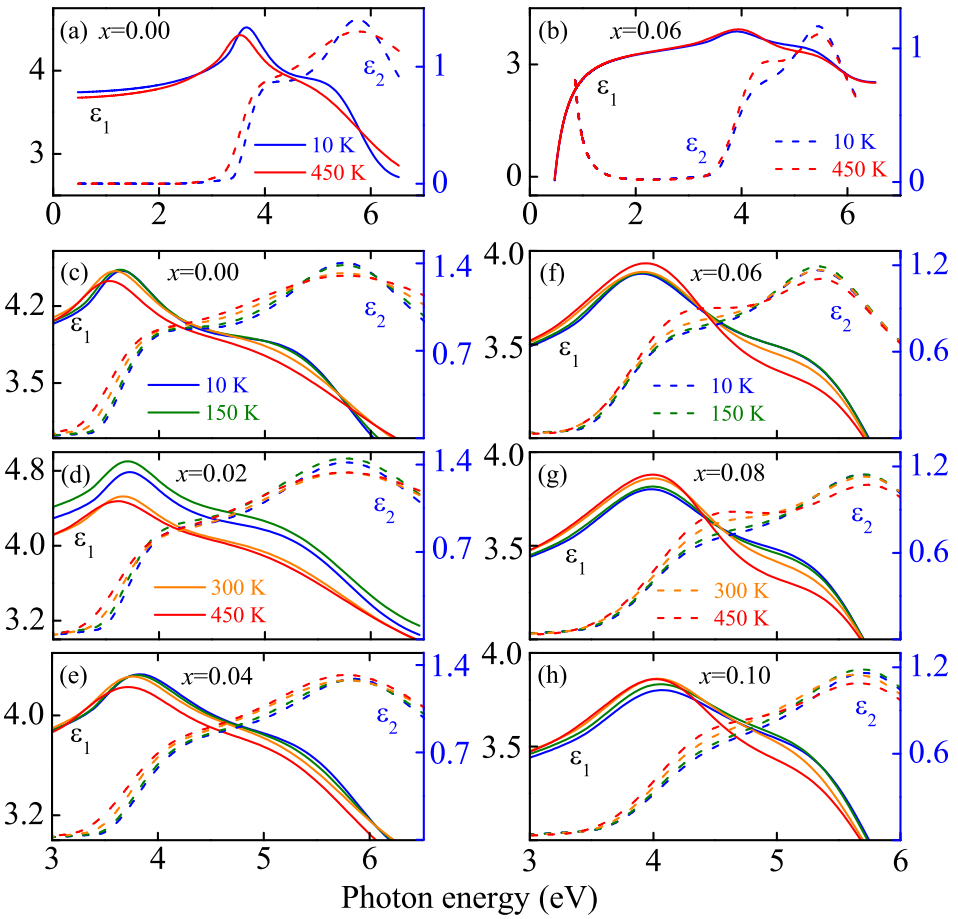

FIG. 2. The real part ε_1 (solid lines) and imaginary part ε_2 (dashed lines) of the dielectric functions for the BLSO films from 10 K to 450 K. Note that the photon energy region is covered from 0.5 to 6.5 eV in (a) and (b), which can present the wide optical dispersion of the BLSO films doped with $x = 0.0$ and 0.06.

temperature is different from the film doped with $x \leq 0.04$ and $x \geq 0.06$. The real and imaginary parts of dielectric function increase with the photon energy and approach the maximum, then decrease upon the photon energy increasing. The critical point is associated with interband electronic transition between the valence and conduction bands. For the film doped with $x \leq 0.04$, two transition regions can be affected by temperature. However, the second transition can be affected only for the film doped with $x \geq 0.06$. Thus, the La concentration of the films affects the energy level of the materials. At lightly doping ($x \leq 0.04$) film, some La ions can substitute for Ba ions and the impurity energy level appears between VBM and CBM. At higher La doping ($x \geq 0.06$) case, the concentration is close to the saturation and the structure basically reaches a stable state. Thus, the excess ions cause little impact on the direct transition.

B. Temperature dependent bandgap energy

Figure 3(a) shows temperature dependence of the bandgap energy for the BLSO films. There has been a significant difference of the trends between $x \leq 0.04$ and $x \geq 0.06$. For the films doped with $x \leq 0.04$, the bandgap shows a sharp decline, corresponding to the temperature increasing from 10 K to 450 K. In particular, it can be found that the bandgap value decreases from 3.95 to 3.41 eV for the film with $x = 0.04$. As can be seen, the temperature has an important role in the variation of the bandgap energy. We can also see that the rate for variation of the bandgap increases with the temperature. With increasing temperature, the longitudinal phonons change the interatomic distance along the direction of their propagation, and the transversal phonons will be perpendicular to their propagation.[23] Thus, the lattice constant of the BLSO films is varied due to the dilatation of lattice and the narrowing of interatomic distances. The variation of the lattice constant results in the modification of the electronic band structure which further moves the conduction band downward and the valence band upward.[24]

Generally, temperature dependence of the bandgap parameter can be described with the Bose-Einstein model, in which the carrier-phonon coupling is taken into account.[25,26] The model can be written as $E_g(T) = E_g(0) - 2a_B/[\exp(\Theta_B/T) - 1]$, here, a_B is the strength of the electron-phonon interaction, and Θ_B is the characteristic temperature representing the effective phonon energy on the temperature scale.[27] The best-fitting parameters are shown in Figs. 3(b) and 3(c). For lightly La doping, the parameters a_B and Θ_B increase linearly with La concentration. For heavily La doping, the parameters do not change with La concentration. For lightly La doping, the bandgap variation is more than 0.5 eV, which is much larger than that (about 0.16 eV) for heavily La doping, as shown in Figure 3(d). On the other hand, the bandgap increases with increasing La doping concentration. For different La concentration, the impact factor of the temperature and La doping concentration on the bandgap energy variation is significantly different, as shown in Figure 4. For La doping concentration at $x \leq 0.04$, there has been an obvious variation. As the La doping concentration increases, there will be more electrons to be coupled with the phonons, which cause the parameter a_B decreasing. According to the Bose-Einstein model, the bandgap energy has a negative correlation with the parameter a_B, which is consistent with the experimental results. At higher La doping ($x \geq 0.06$), there is a significant increase of bandgap energy, which can be explained by the Burstein-Moss effect due to the degenerate nature of the films.[28,29] As the carrier concentration exceeds the Mott critical density of BLSO, the bottom of the conduction band will be filled. Thus, more energy is needed to excite the electrons from the donor impurity band to the conduction band, resulting in an optical bandgap widening.[30] For $x = 0.06$, 0.08, and 0.10, the bandgap energy still increases with the temperature, but the variation is much less than that for the La doping concentration at $x \leq 0.04$. The bandgap energy is relatively stable with temperature. This shows that at a highly doping concentration, the electronic band and optical properties almost unchanges with the temperature or La concentration, which can be seen from the parameters a_B and Θ_B.

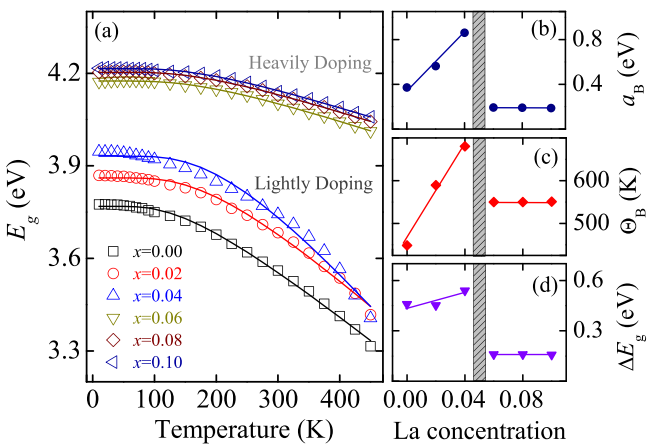

FIG. 3. (a) Temperature dependence of bandgap energy for the BLSO films with different La concentration. The solid lines correspond to the fitting from Bose-Einstein model. The best-fitting parameters (b) a_B and (c) Θ_B of the Bose-Einstein model as a function of doping concentration. (d) The bandgap discrepancy is varied with the La concentration.

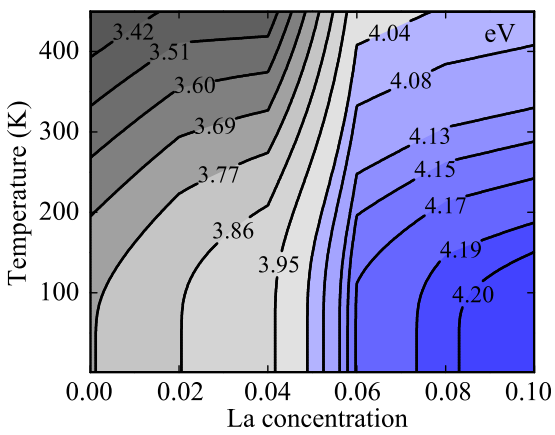

FIG. 4. A two-dimensional picture based on the bandgap energy variation with the temperature and La concentration. The numbers correspond to the bandgap energy and the unit is "eV".

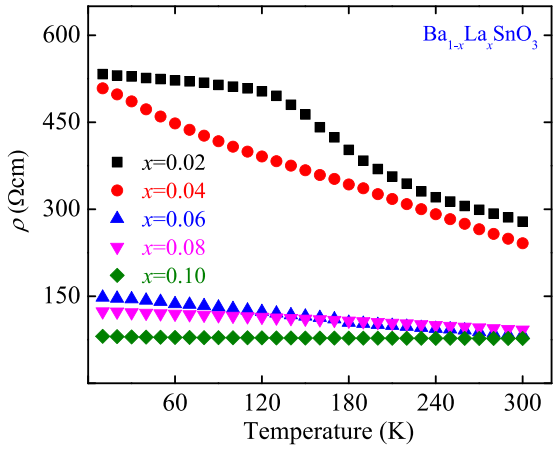

FIG. 5. Temperature dependent resistivity for the BLSO ($x = 0.02$–0.10) films. Note that the film doped with $x = 0.00$ is not measured because the undoped BSO film is insulating.

C. Electrical resistivity analysis

To further understand the intrinsic characteristics of the BLSO films, temperature dependence of electrical resistivity is shown in Figure 5. Note that the undoped film is not measured because it is insulating. The resistivity decreases systematically with increasing the temperature from $x = 0.02$ to 0.04. It is due to the fact that there have been more free carriers excited from the donor impurity band to the conduction band by the thermal excitation. However, it becomes almost constant for $x \geq 0.06$, indicating that there is a weak temperature dependence for heavily La doping. The resistivity in BLSO films is dominated by scattering such as grain boundary scattering and ionized-dopant scattering. As the carrier concentration exceeds the Mott critical density of BLSO films, the Fermi level moves up into the conduction band, which results in a metallic behavior.[31] It shows that the energy levels created by substitution of lanthanum for barium are not significantly stabilized with respect to the bottom of the conduction band. The variation of the resistivity with the temperature and La concentration shows a similar pattern with the bandgap variation, which suggests that the doping concentration of BLSO films tends to a saturated state.

D. Electronic transition origin

The bandgap variation with La concentration can be explained by the lattice expansion. As we know, the bandgap value of a semiconductor is dependent on the position and width of the conduction band and valence band. The undoped BSO has an ideal cubic perovskite structure with the Sn-O-Sn bond angle of 180°. The top of the valence band depends on the contributions of the O 2*p* orbitals and the bottom of the conduction band is predominantly composed of nonbonding Sn 5*s* orbitals.[32] The ionic radius of La^{3+} ion is around 0.103 nm, which is less than that of Ba^{2+} (0.135 nm).[33] Generally, the lattice spacing decreases with increasing the content of a smaller ion. However, there has been an unusual lattice expansion for La introduction, as shown in Fig. 6. With La^{3+} ion doped in BSO, it provides electron states inside the conduction band of BSO, which is mainly characterized as the Sn 5*s* states with a Sn-O antibonding character. It means that a La ion acts as an electron donor and its ionic valence becomes La^{3+}. The occupation in the antibonding state can cause repulsive force between Sn and O. It reduces the total energy of the crystal structure, which results in the expansion of the lattice.[14] The Sn-O bond length caused by the lattice expansion has been stretched. The electrons need to gain more energy to transit

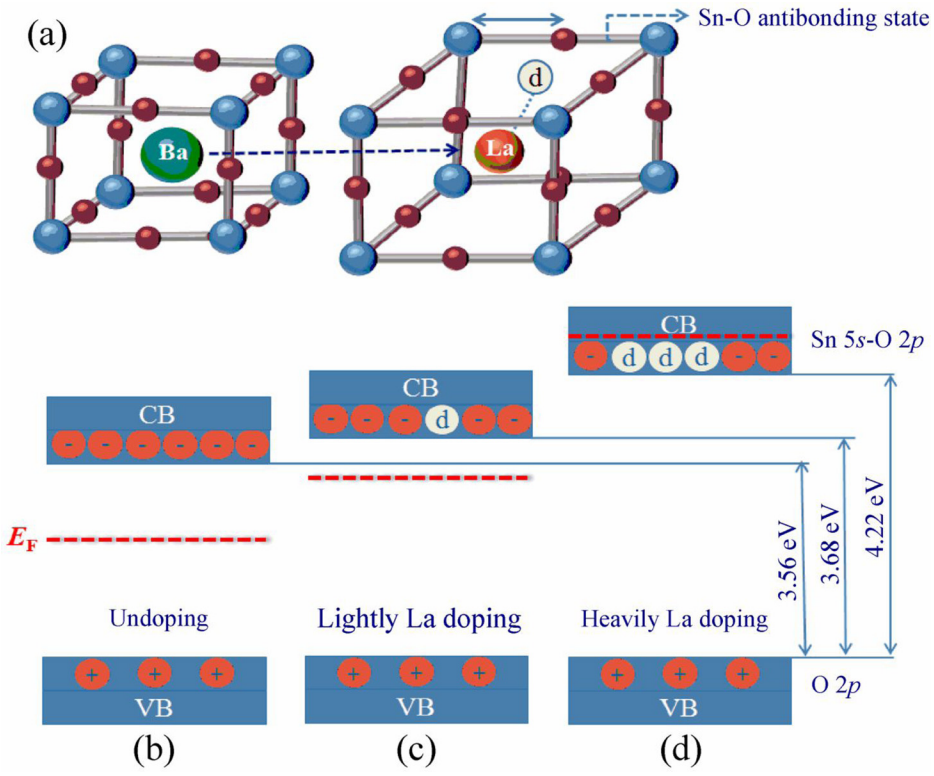

FIG. 6. (a) The cubic structure of the BSO material and the occupation in the Sn-O antibonding state caused by La ion. Schematic representation of the electronic band structure for the BLSO films with the La concentration of (b) 0%, (c) 2%, and (d) 10%, respectively. The parameter E_F denotes the Fermi energy level. Note that the symbols (+) and (−) indicate the intrinsic holes and electrons. The symbol "ⓓ" indicates the electrons induced by the La-doping.

from O 2*p* to Sn 5*s*, which explains the increase of the bandgap energy. The La *d* orbital energy is high, and the CBM of BSO has little contribution from Ba ions. Thus, the substitution on the Ba causes little impact on the CBM.[22] Figs. 6(b)–6(d) show schematic representation for the electronic band structure of the BLSO films with La concentration of 0%, 2%, and 10%. For the undoped BSO, the Fermi level is closed to the bandgap midline. The increment of La concentration would induce the increase of electron carrier, which results in the form of the tail state in the bottom of conduction band. The Fermi level moves up with the increase of La concentration, and the bandgap energy shows s blue-shift. For heavily La doping, it induced the Fermi energy level going into the conduction band, and formed the Burstein-Moss effect. Each substitution for Ba ion can donate an electron inside the conduction band of the BLSO. Also, the Fermi level was formed in the conduction band as the doped La atom can donate an electron carrier to the conduction band by the ionization. It leads to the degenerate semiconducting behavior of the material.

For higher La doping ($x \geq 0.06$), the Fermi level moves up into the conduction band, thus causing the electron hopping hardly from the minimal energy level to the VBM. It results in a significant increase in the bandgap. The minimal band energy is expanded obviously with the La doped with $x \geq 0.06$. As mentioned before, there are two transitions at Γ point and R point for the BLSO films. As for heavily La doping, the Fermi level is above the CBM at Γ point. Thus, the first absorption E_{01} has a very little probability of occurrence and the electrons can only be excited from the valence band to the conduction band at the R point. The bandgap energy is around 4.0–4.3 eV for heavily La doping, which is consistent with the transition energy at the R point. Meanwhile, the doping concentration may tend to a saturated state. The excess La^{3+} has little chance to replace Ba^{2+}. Thus, the trend of lattice expansion has a large decrease. The temperature and La concentration cause little impact on the lattice expansion and/or bandgap energy variation. Recently, high quality $CuGa_{0.8}Cr_{0.2}O_2$ films (a kind of *p*-type TCOs) has been grown by chemical solution technique.[34] Its Fermi level is above the top of the valence band. A prototype of *pn* junction can be composed by *n*-type BLSO and *p*-type $CuGa_{0.8}Cr_{0.2}O_2$. The *pn* junction shows a great potential to realize the photoelectric interaction. For example, it may be used in fully transparent circuit and transparent solar cells.

IV. SUMMARY

In summary, we report transparent and conductive La-doped BSO films with La concentration at $x = 0$–0.10 deposited on (0001) sapphire substrates by a sol-gel method. The films exhibit a high transmittance with more than 80% in the visible region. To further understand the optical properties and bandgap energy of BLSO films, the dielectric functions were uniquely extracted by fitting the transmittance spectra in the photon energy of 0.5–6.5 eV from 10 K to 450 K. It was found that the absorption edge of the BLSO films presents a red-shift trend with the temperature. The dielectric function shows that there have been two obvious electronic transitions in BLSO (around 3.5 eV and 4.5 eV). It is interesting to be found that the effect of temperature on the variation of bandgap energy and transmittance spectra is different between lightly doping ($x \leq 0.04$) and heavily doping ($x \geq 0.06$). Because of an unusual expansion, there has been a limit of the solid solution for the La^{3+} ion in BSO, which is not common in ion doped materials. Thus, there has been a saturated doping concentration for this material system. For heavily doping, BLSO behaves as a degenerate semiconductor, which has an obvious variation with the physical properties of lightly doping BLSO. The variation of the resistivity shows a similar pattern with the bandgap, which is consistent with the results.

ACKNOWLEDGMENTS

This work was financially supported by Major State Basic Research Development Program of China (Grant Nos. 2011CB922200 and 2013CB922300), the Natural Science Foundation of China (Grant Nos. 11374097 and 61376129), Projects of Science and Technology Commission of Shanghai Municipality (Grant Nos. 14XD1401500, 13JC1402100, and 13JC1404200), and the Program for Professor of Special Appointment (Eastern Scholar) at Shanghai Institutions of Higher Learning.

[1]G. Thomas, Nature **389**, 907 (1997).
[2]K. Hayashi, S. Matsuishi, T. Kamiya, M. Hirano, and H. Hosono, Nature **419**, 462 (2002).
[3]C. H. Ahn, J. M. Triscone, and J. Mannhart, Nature **424**, 1015 (2003).
[4]O. Auciello, J. F. Scott, and R. Ramesh, Phys. Today **51**(9), 22 (1998).
[5]B. N. Mbenkum, N. Ashkenov, M. Schubert, M. Lorenz, H. Hochmuth, D. Michel, M. Grundmann, and G. Wagner, Appl. Phys. Lett. **86**, 091904 (2005).
[6]K. Dörr, J. Phys. D: Appl. Phys. **39**, R125 (2006).
[7]L. Geske, V. Lorenz, T. Muller, L. Jager, H. Beige, H. P. Abicht, and V. Mueller, J. Eur. Ceram. Soc. **25**, 2537 (2005).
[8]U. Lampe, J. Gerblinger, and H. Meixner, Sens. Actuators, B **26**, 97 (1995).
[9]S. W. Tao, F. Gao, X. Q. Liu, and O. T. Sørensen, Sens. Actuators, B **71**, 223 (2000).
[10]U. Lampe, J. Gerblinger, and H. Meixner, Sens. Actuators, B **18**, 132 (1994).
[11]S. V. Manorama, C. V. G. Reddy, and V. J. Rao, Appl. Surf. Sci. **174**, 93 (2001).
[12]Y. F. Zhang, H. R. Zhang, Y. F. Wang, and W. F. Zhang, J. Phys. Chem. C **112**, 8553 (2008).
[13]Y. Z. Wang, E. Bevillon, A. Chesnaud, G. Geneste, and G. Dezanneau, J. Phys. Chem. C **113**, 20486 (2009).
[14]H. J. Kim, U. Kim, T. H. Kim, J. Kim, H. M. Kim, B. Jeon, W. Lee, H. S. Mun, K. T. Hong, J. Yu, K. Char, and K. H. Kim, Phys. Rev. B **86**, 165205 (2012).
[15]X. Luo, Y. S. Oh, A. Sirenko, P. Gao, T. A. Tyson, K. Char, and S.-W. Cheong, Appl. Phys. Lett. **100**, 172112 (2012).
[16]C. Shan, T. Huang, J. Z. Zhang, M. J. Han, Y. W. Li, Z. G. Hu, and J. H. Chu, J. Phys. Chem. C **118**, 6994 (2014).
[17]C. Shan, P. Chang, K. Shi, Y. W. Li, Z. G. Hu, and J. H. Chu, RSC Adv. **04**, 34987 (2014).
[18]T. N. Stanislavchuk, A. A. Sirenko, A. P. Litvinchuk, X. Luo, and S.-W. Cheong, J. Appl. Phys. **112**, 044108 (2012).
[19]G. E. Jellison and F. A. Modine, Appl. Phys. Lett. **69**, 371 (1996).
[20]H. Y. Fan, Phys. Rev. **82**, 900 (1951).
[21]S. Sallis, D. O. Scanlon, S. C. Chae, N. F. Quackenbush, D. A. Fischer, J. C. Woicik, J.-H. Guo, S. W. Cheong, and L. F. J. Piper, Appl. Phys. Lett. **103**, 042105 (2013).
[22]H. R. Liu, J. H. Yang, H. J. Xiang, X. G. Gong, and S. H. Wei, Appl. Phys. Lett. **102**, 112109 (2013).
[23]S. Biernacki, U. Scherz, and B. K. Meyer, Phys. Rev. B **49**, 4501 (1994).

[24]B. S. Li, Y. C. Liu, Z. Z. Zhi, D. Z. Shen, Y. M. Liu, J. Y. Zhang, and X. W. Fan, J. Cryst. Growth **240**, 479 (2002).
[25]M. J. Han, K. Jiang, J. Z. Zhang, Y. W. Li, Z. G. Hu, and J. H. Chu, Appl. Phys. Lett. **99**, 131104 (2011).
[26]W. W. Li, K. Jiang, J. Z. Zhang, X. G. Chen, Z. G. Hu, S. Y. Chen, L. Sun, and J. H. Chu, Phys. Chem. Chem. Phys. **14**, 9936 (2012).
[27]M. Beaudoin, A. J. G. DeVries, S. R. Johnson, H. Laman, and T. Tiedje, Appl. Phys. Lett. **70**, 3540 (1997).
[28]E. Burstein, Phys. Rev. **93**, 632 (1954).
[29]T. S. Moss, Proc. Phys. Soc. London, Sect. B **67**, 775 (1954).
[30]Q. Z. Liu, J. J. Liu, B. Li, H. Li, G. P. Zhu, K. Dai, Z. L. Liu, P. Zhang, and J. M. Dai, Appl. Phys. Lett. **101**, 241901 (2012).
[31]S. Michael and T. Ashutosh, J. Appl. Phys. **101**, 124912 (2007).
[32]H. Mizoguchi, H. W. En, and P. M. Woodward, Inorg. Chem. **43**, 1667 (2004).
[33]R. D. Shannon, Acta Crystallogr. A **32**, 751 (1976).
[34]M. J. Han, K. Jiang, J. Z. Zhang, W. L. Yu, Y. W. Li, Z. G. Hu, and J. H. Chu, J. Mater. Chem. **22**, 18463 (2012).